Prepared For

Jet Propulsion Laboratory

Contract No. 950252

JET PROPULSION LABORATORY
CALIFORNIA INSTITUTE OF TECHNOLOGY
PASADENA, CALIFORNIA

THERMAL MODELING OF
A SIMULATED JPL SPACECRAFT
PHASE I RESULTS

Prepared For

Jet Propulsion Laboratory

Contract No. 950252

by

Frank Gabron

Arthur A. Fowle

C-64924

TABLE OF CONTENTS

LIST OF FIGURES

LIST OF TABLES

SUMMARY

Dimensionless groups of thermal modeling parameters were derived to identify methods for testing reduced-scale thermal models and predicting from those experiments the thermal characteristics of full-scale spacecraft vehicles or components. The following heat transfer phenomena were considered in the analysis:

1. Heat transport by solid conduction;
2. Heat transport at solid-to-solid interfaces;
3. Heat generated by internal power sources;
4. Internal energy changes during transients;
5. Heat transport via thermal radiation emitted from surfaces;
6. Heat transport via radiation absorbed at surfaces.

Two sets of scaling laws for thermal modeling were derived from the controlling dimensionless groups. One set would require that the temperature-time distributions (in normalized space) of model and prototype be identical. This could be accomplished by fabricating the model and prototype of different materials. Another set would require that the model and prototype be made of identical materials. In this case the temperatures in the model and prototype would differ.

We have attempted to identify a most promising method for thermal modeling; however, we find that each method has merits which may be ideally

suited to the thermal modeling of a certain spacecraft, and the design of each different prototype will have to be evaluated in order to select the best method. For example, in certain prototype systems it may not be possible to test a reduced-scale thermal model with identical temperatures, at corresponding geometric locations, if the thermal conductivity of the prototype is extremely small. Similarly, it may not be feasible to test a thermal model fabricated from the same material as the prototype if the surface characteristics or the thermal properties are highly temperature dependent. In addition, the scale may be limited by the highest absolute temperature level tolerable in the model and test chamber.

Two thermal models (one approximately half scale) were fabricated in accordance with the scaling law which would predict equivalent temperatures at identical geometric locations. The model temperature distributions were measured in a "cold" (LN_2 temperature) wall vacuum chamber. The details of the test results and the apparatus are presented in Sections II and III of this report.

The results of the tests indicate that the thermal modeling concept adopted for this program is practical; however, we encountered some experimental difficulties with the small models used in this program. In the smallest scale model the input power dissipated was of the order of 700 milliwatts, and for this input power range one must be concerned with the effects of instrumentation and power leads. Uncertainties in the heat flow

characteristics of such leads thus influence the experimental accuracy of thermal modeling on such a small scale.

In summary, we believe that precise thermal modeling is inherently limited by the size of the smallest scaled model (as measured by the input power per unit volume). If it is necessary to conduct thermal modeling experiments and obtain a high degree of accuracy at low input power levels, further work will be required to identify and eliminate the uncertainties involved in instrumenting the test models.

INTRODUCTION

The basic objective of our program is to investigate methods for predicting the thermal performance of a full-scale spacecraft package or its components from ground testing of reduced-scale models. The subject material contained in this report deals with the first phase of an over-all program which entails the testing of scale models of a simulated spacecraft. The purpose of this Phase I effort is to evaluate approaches to the thermal modeling problem and to devise and undertake certain basic experiments to evaluate the thermal modeling laws proposed for future phases.

This program is being funded by the Jet Propulsion Laboratory of the California Institute of Technology. The Technical Representative of the Jet Propulsion Laboratory for this program is Dr. J. F. Vickers.

ACKNOWLEDGEMENTS

The authors wish to thank Mr. Peter F. Strong of the Research and Development Division for his helpful suggestions during the course of this work.

Mr. P. Murphy of the Engineering Division assembled the experimental apparatus and completed the testing of the thermal models. His painstaking care in insulating, instrumenting, and assembling the test models contributed significantly to the program.

THERMAL MODELING OF A SIMULATED JPL SPACECRAFT
PHASE I RESULTS

I. THE THERMAL MODELING PROBLEM

A. INTRODUCTION

The basis for modeling any physical system must be the derivation of the independent dimensionless groups containing (together) all the physical quantities which interact to determine the behavior of this system. Once having determined the functional relationship between the dimensionless groups by analysis or experiment the physical behavior of all similar systems is completely characterized. The advantages of this approach stem from the fact that the independent variables controlling the behavior of the system are reduced to a minimum, and, in cases where experiment is required to determine the behavior, tests at a reduced geometric scale can be used to predict the behavior of a larger system.

The least number of dimensional quantities needed to describe the system and its interaction with its environment must be determined by physical reasoning. This implies, and requires, an understanding of the active physical phenomena.

In the case of the thermal modeling of spacecraft we are concerned with the temperature distributions which result from internal power sources and the thermal interaction of the craft with its environment. Although closed-cycle thermodynamic systems involving flow loops and power

machinery may be present in many spacecraft, we confine our attention to spacecraft elements wherein the temperature distributions are determined by heat transfer via the mechanisms of radiation and conduction in solid members. In order to derive the dimensional quantities which determine the thermal behavior of this class of spacecraft system it is useful to think in terms of the following active heat transfer phenomena:

1. Heat transport by solid conduction
2. Heat transport at solid-to-solid interfaces
3. Heat generated by internal sources
4. Heat (internal energy) changes during transient
5. Heat transport via radiation emitted from surfaces
6. Heat transport via radiation absorbed at surfaces

B. HEAT TRANSPORT BY SOLID CONDUCTION

Heat transfer by solid conduction can be characterized by the thermal conductivities of the materials of the system, K, and by the temperature distributions in these materials which introduce the variables, L, and T. For a single thermal conductivity value to be sufficient, the materials must be isotropic. If the thermal conductivities of the materials of the system are themselves temperature dependent, then the dimensional quantities which describe this dependence enter.

C. HEAT TRANSPORT AT SOLID-TO-SOLID INTERFACES

Heat transfer at solid-to-solid interfaces when considered on a macroscopic scale introduces the concept of thermal resistance or its reciprocal, thermal contact conductance, C. The thermal contact conductance is defined as the ratio of the heat transfer across the interface per unit of the superficial contact area and temperature difference across the contact gap. It is well known that the value of the thermal contact conductance for systems in vacuo depend on the structural characteristics of the joining materials, on their surface finish, and on the contact pressures.

D. HEAT GENERATED BY INTERNAL SOURCES

In typical spacecraft components, sources of internal heat exist due to the I^2R losses in the electric circuitry. In recognition of these internal sources it is convenient to introduce a parameter, q^*, which is the internal power generated per unit of volume. The real spacecraft electronic component may be made up of a non-homogeneous mixture of materials and a practical question will always exist as to the linear scale on which model similarity is to be preserved.

E. INTERNAL ENERGY CHANGES DURING TRANSIENTS

Consideration of the requirements for thermal similitude in non-steady-state systems introduces the thermal inertia properties of the system and time, τ. The thermal inertia of the system is simply

characterized by the produce of density, ρ , and specific heat, C_p, of the materials from which it is constituted.

F. HEAT TRANSPORT via EMITTED RADIATION

The total emissive power per unit of area of the surfaces making up the system is given by the product of the total hemispherical emittance of the surface, ϵ, the Stefan-Boltzmann constant, σ , and the fourth power of its absolute temperature. Therefore, consideration of emitted radiation introduces the new factors, ϵ, and σ . The total hemispherical emittance, ϵ, is the only factor over which we have experimental control. For any particular surface, ϵ, varies with its temperature and surface condition - degree of roughness, oxidation, contamination, etc. In addition, ϵ, is a doubly-integrated quantity involving ϵ_λ , the monochromatic emittance and ϵ_θ, the directional emittance. The latter factors become important only when we consider the intensity and spectral distribution of the radiant flux incident on the surface.

G. HEAT TRANSPORT via ABSORBED RADIATION

The radiant heat absorbed at a surface per unit area is the product of its absorptance, α , and the incident flux, $\emptyset$. The absorptance depends on the factors affecting emittance (surface temperature, condition and direction) and, in addition, on the characteristics of the incident radiation measured by its distribution in the spectrum. For this reason,

it is useful to separate the flux incident on the surface elements of the spacecraft system into components identified by source.

One contribution to the total flux is that which originates within the system by virtue of the fact that all exposed surfaces of the system are themselves emitters. The flux from these internal sources falling at any specified surface is a portion of the sum of the reflected and emitted radiation issuing from all the surfaces that the element in question can "see". This portion depends on the geometry of the system and on the angular distribution of the radiant energy leaving the "viewed" surfaces. If the intensity of this leaving energy (both emitted and reflected) obeys a known law, such as Lambert's cosine law, then the portion incident can be predicted on the basis of geometry only. The magnitude of the flux issuing from the "viewed" internal sources depends on the emissive power of these surfaces (hence, $\epsilon \sigma T^4$) and the reflected power. The reflected power, in turn, depends on emissive power of all surfaces, on the geometry and on the absorptance of all surfaces. In summary, we reason that the absorbed energy depends on the geometry and on the emissive power and absorptance of all surfaces.

The other contributions to the total incident flux are characterized by sources lying outside the system; for instance, sunlight, and reflected or direct radiation from the moon and planets. The influence of

each external source must be accounted for by introducing additional variables. ϕ_{01}, ϕ_{02}, ϕ_{03}, etc., might be used to denote the intensity of the radiant energy from the various external sources, and α_{01}, α_{02}, α_{03}, etc., might be used to denote the absorption characteristics of the surfaces of the system to these incident radiations. Of course, an additional requirement for rigorous thermal similitude is that the direction of the radiant flux from external sources is the same in model and prototype.

H. FORMATION OF DIMENSIONLESS GROUPS

From the previous discussion one notes that the thermal behavior of spacecraft is determined by a very extensive number of dimensional parameters, and this fact may make thermal modeling for the general case impractical if not impossible. However, the application of certain reasonable restraints can make the problem of thermal modeling tractable.

First, we restrict consideration to model and prototype systems for which the K's, ρ's, C_p's, α's and ϵ's can be considered temperature independent, and, second, to solid materials that can be considered isotropic conductors. Third, to eliminate the influence of the spectral and angular distribution on the emitted and absorbed radiation, we restrict consideration to model and prototype systems which have the same surface characteristics.

With these restrictions a single notation for K, ρ, α, etc., is sufficient for the development of the thermal modeling factors*.

The formation of the controlling dimensionless groups (often referred to as the π groups) may be accomplished in a number of ways. Formal procedures are described in the literature. We prefer a method which points up the physical significance of the π's. Thermal similitude requires that the heat transport and internal energy changes be proportional in model and prototype. To state this condition mathematically we proceed as follows. First, we express the heat transfer and energy change effects in dimensional terms:

Effect	Dimensional Statement	
Heat Flux via Solid Conduction	$\frac{KT}{L}$	(watts/cm^2)
Heat Flux at Solid-to-Solid Interface	CT	"

*It might be noted that the restrictions listed are not necessary in order to make the thermal modeling of all systems practical. Some of these restrictions may be removed for certain relatively simple thermal systems or components of a total system without making thermal modeling impractical.

(Cont'd) Effect	Dimensional Statement	
Heat Flux Due to Internal Sources	$q^* L$	(watts/cm^2)
Heat Flux Due to Changing Internal Energy	$\frac{\rho C_p T L}{\tau}$	"
Heat Flux via Emitted Radiation	$\epsilon \sigma T^4$	"
Heat Flux via Absorbed Radiation (Internal Sources)	$\alpha_T \phi_T$	"
Heat Flux via Absorbed Radiation (External Sources)	$\alpha_{01} \phi_{01} \alpha_{02} \phi_{02}$, etc.	"

Now, taking ratio's with respect to the heat flux due to solid conduction, we get

$$\pi_1 = \frac{CL}{K}$$

$$\pi_2 = \frac{q^* L^2}{KT}$$

$$\pi_3 = \frac{\rho C_p L^2}{K \tau}$$

$$\pi_4 = \frac{\epsilon \sigma T^3 L}{K}$$

$$\pi_5 = \frac{\alpha_T \phi_T L}{KT}$$

$$\pi_6, \pi_7, \text{etc} = \frac{\alpha_{01} \phi_{01} L}{KT}, \frac{\alpha_{02} \phi_{02} L}{KT}, \text{etc.}$$

As the temperature, T, appears in a number of the above-listed π's, and as temperature can be considered a dependent variable in the

experimental model studies, a more convenient set can be gained by rearrangement as follows:

$$\pi_1 = \frac{CL}{K}$$

$$\pi_2 = \frac{q^* L^2}{KT}$$

$$\pi_3 = \frac{\rho C_p L^2}{K \tau}$$

$$\pi_4 = \frac{\epsilon \sigma q^{*3} L^7}{K^4}$$

$$\pi_5 = \frac{\alpha_T \phi_T}{\epsilon \sigma T^4}$$

$$\pi_6, \pi_7, \text{ etc.} = \frac{\alpha_{01} \phi_{01}}{q^* L}, \frac{\alpha_{02} \phi_{02}}{q^* L}$$

A useful set of scaling laws for model testing would specify that the temperature-time distributions in normalized space would be identical in model and prototype. In addition, we have the restriction that the emittance and absorptance of corresponding surfaces in model and prototype are identical. In this instance, for thermal similitude

$$\frac{C_m L_m}{K_m} = \frac{C_s L_s}{K_s}$$

$$\frac{q^*_m L^2_m}{K_m} = \frac{q^*_s L^2_s}{K_s}$$

$$\frac{\rho_m C_{pm} L^2_m}{K_m} = \frac{\rho_s C_{ps} L^2_s}{K_s}$$

$$\frac{q^{*3}_m L^7_m}{K^4_m} = \frac{q^{*3}_s L^7_s}{K^4_s}$$

$$\pi_{5m} = \pi_{5s} \text{ (identically satisfied)}$$

$$\frac{\phi_{01\,m}}{q^*_m L_m}, \quad \frac{\phi_{02\,m}}{q^*_m L_m}, \quad \text{etc.} = \frac{\phi_{01s}}{q^*_s L_s}, \quad \frac{\phi_{02s}}{q^*_s L_s}, \quad \text{etc.}$$

or

$$\frac{L_m}{K_m} = \frac{L_s}{K_s}$$

$$C_m = C_s$$

$$q^*_m L_m = q^*_s L_s$$

$$\rho_m C_{pm} L_m = \rho_s C_{ps} L_s$$

$$\phi_{01m}, \phi_{02m}, \text{etc.} = \phi_{01s}, \phi_{02s}, \text{etc.}$$

It is this last set of scaling laws which we have examined experimentally in the Phase I of the subject contract. As these experiments were made at steady state, the thermal inertia characteristics of the models do not enter the problem. In addition, ϕ_{01}, ϕ_{02}, etc., were made negligible in the design of the experimental apparatus. In summary, we would predict the same temperature at corresponding points if

$$\frac{L_m}{K_m} = \frac{L_s}{K_s}$$

$$C_m = C_s$$

$$q_m^* L_m = q_s^* L_s$$

Other possibilities certainly exist and deserve attention. For instance, suppose it is convenient to make the model and prototype of identical materials. Suppose further, we place the additional restriction that the radiation characteristics of corresponding surfaces in model and prototype are identical. Then, in this case

$$C_m L_m = C_s L_s$$

$$\frac{L_m^2}{\tau_m} = \frac{L_s^2}{\tau_s}$$

$$q_m^* L_m^{7/3} = q_s^* L_s^{7/3}$$

$$T_m L_m^{1/3} = T_s L_s^{1/3}$$

$$\pi_{5m} = \pi_{5s}$$

$$\phi_{01m} L_m^{4/3}, \phi_{02m} L_m^{4/3}, \text{ etc.} = f_{01s} L_s^{4/3}, \phi_{02s} L_s^{4/3}, \text{ etc.}$$

The above laws, of course, hold only when the properties of the model and prototype are independent of temperature.

II. THERMAL MODELS AND TEST EQUIPMENT

A. INTRODUCTION

During this Phase I test program we designed an experiment to investigate the validity of the thermal modeling laws derived in Section I. The objective was to construct and test thermal models, at steady-state conditions, which would embody those heat transfer mechanisms present in the later Phases of the subject program. In particular, it was derived to investigate conductive and radiative effects without the added complexity of convective heat transfer.

A "basic" thermal model and two scale models were designed and built. One scale model was designed in accordance with the set of modeling laws which predict equivalent temperatures at identical geometrical locations using different model materials. The other scale model was designed in accordance with the laws which predict scaled temperatures at equivalent geometric locations when the model and scale model are made of identical materials.

In the following sections we will describe the experiments and results obtained with a scale model constructed of a different material than the "basic" thermal model. We had planned to complete the testing of a scale model constructed of the same material as the "basic" model; however, this effort was regarded as of secondary importance since the proposed

Phase II program would involve testing of basic and scale models of different materials.

B. THERMAL MODEL DESIGN

The objective of the Phase I experiments was to devise and test a set of simple thermal models which would validate the thermal modeling theory and yet embody the heat transport mechanisms which would be involved in our future work in Phase II. In addition, it was desired to test models of relatively small dimensions in a simple inexpensive vacuum chamber. The basic model design incorporated the following heat transfer mechanisms:

1) Heat transport by solid conduction
2) Heat transport at solid-to-solid interfaces
3) Heat generated by internal sources
4) Heat transport via emitted surface thermal radiation

We thus eliminated, in part, the effects of absorbed fluxes from the environment (by testing the models in a vacuum chamber whose "black" walls were maintained at liquid nitrogen temperature) and the effects of internal energy changes during transients (by testing at steady-state conditions).

A sketch of the thermal model configuration is shown in Figure 1. Basically, the model resembled a "fin", heated at one end by the dissipation

MODEL NO.	MATERIAL			DIMENSIONS (IN.)					THERMAL CONDUCTIVITY @10°C "K" WATTS/CM °K
	PT. A	PT. B	PT. C	L0	L2	L3	t	b	
1	ARMCO IRON	POLYVINYL CHLORIDE	ARMCO IRON	3.00	0.75	5.00	0.187	1.25	0.741
2	SAE 4130	POLYVINYL CHLORIDE	SAE 4130	1.411	0.75	2.362	0.088	0.590	0.350

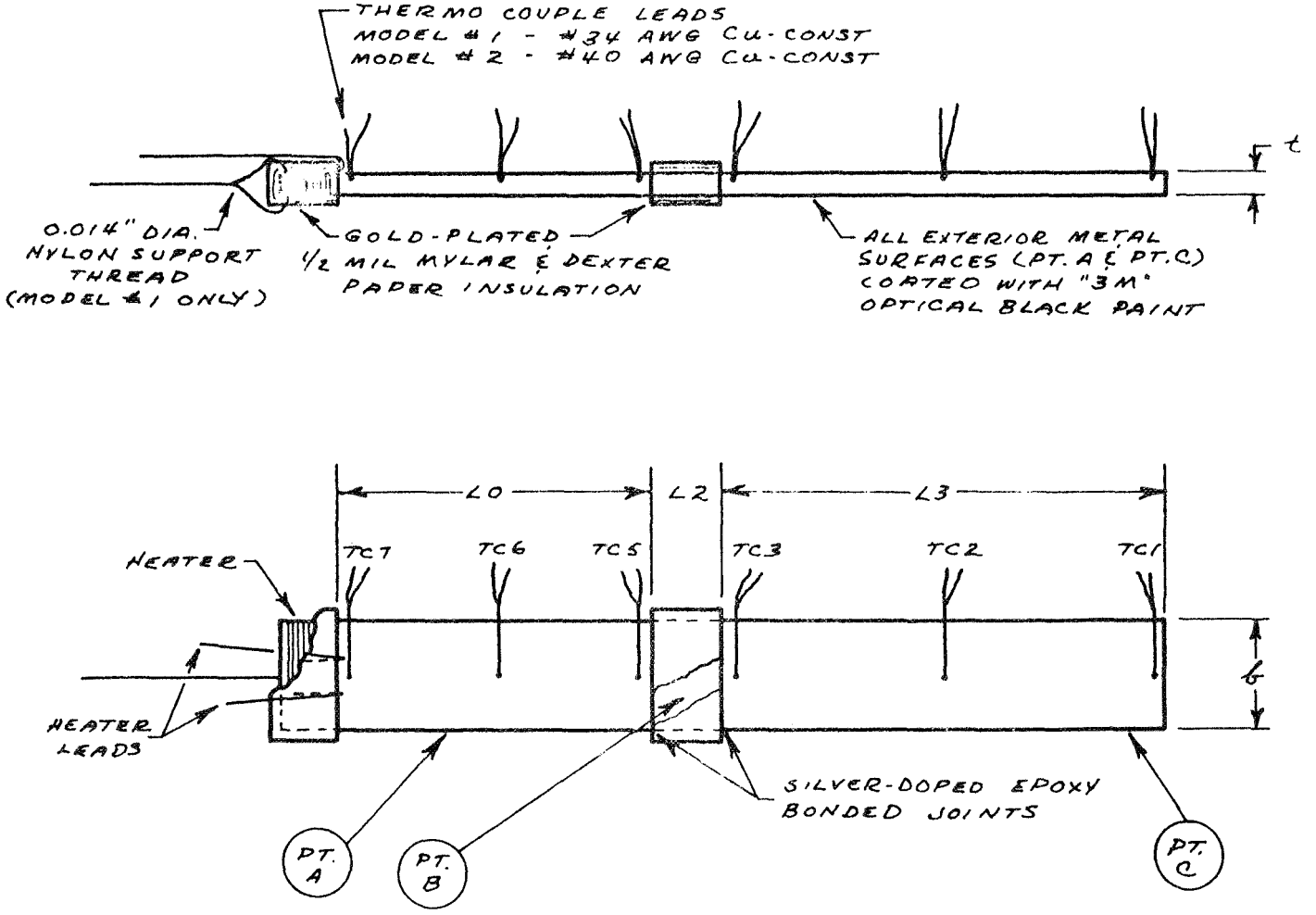

TEST MODEL ASSEMBLY

FIGURE 1

of electrical power. To simulate a solid-to-solid interfacial thermal resistance, a material of low conductivity was bonded between two members having a higher conductivity thereby imposing a large temperature gradient in the fin. This would resemble the physical situation where a heat-conducting path was disturbed by a joint or interface having a low thermal conductance. As shown in Figure 1, the heater was insulated, as was the simulated contact resistance. In this manner the internal power generated would be radiatively dissipated from the surface between the heater and the insulated contact resistance and from the surface between the heater and the insulated contact resistance and the end of the model. This situation would thereby preclude the need for measuring the temperatures of the heater elements themselves to account for any power re-radiated from the heater end. The exposed surfaces of the two models were coated with an "optical black" paint in an attempt to maintain similar surface characteristics since one of the elements of the modeling laws would require that the emittances of the models be similar. Although we could have used other surface coatings with a lower emittance, our experience with this high emittance paint indicates that the uncertainty involved in assuming that the emittances of both models were similar would be ± 0.01. The simulated contact resistance was insulated to prevent radiative effects from altering the effective conductance of the element. That is, the simulated contact resistance members were scaled to have similar conductances in both models and to accomplish this it is necessary to exclude heat transfer by radiation at the surfaces.

The basic model, herein referred to as Model #1, was constructed of Armco iron, a relatively pure iron whose thermal conductivity is known accurately over a wide temperature range and is recognized as a thermal conductivity standard. The simulated contact resistance was fabricated of rigid, polyvinylchloride which has a relatively low thermal conductivity. In Section I it was shown that thermal modeling for identical temperature distributions in model and prototype would satisfy the following laws (provided that the total hemispherical emittance and the absorbed fluxes are similar):

$$\frac{L_1}{K_1} = \frac{L_2}{K_2}$$

$$C_1 = C_2$$

$$q_1^* L_1 = q_2^* L_2$$

Since it was desired to reduce the dimensions of the scale model to make it approximately 1/2 scale, SAE 4130 - a chrome-moly steel having a conductivity of roughly 1/2 that of the Armco iron was used for Model #2. In particular, we calculated the appropriate dimensional ratios by arbitrarily using published conductivity values at $+10^{\circ}C$. The conductivity values are:

SAE 4130 - $K_2 = 0.35$ watts/cm$^{\circ}$K Reference 1

Armco - $K_1 = 0.741$ watts/cm$^{\circ}$K Reference 2

It should be noted that the conductivity ratio of these two materials is somewhat temperature dependent, so that some error is introduced when the temperature level of the models is varied. For these materials the

conductivity ratio varies as follows:

Temperature	K_2/K_1
-50 C	0.435
0 C	0.469
+10 C	0.472
50 C	0.489

This variation of $\pm$ 5 percent over a 100°C range will introduce errors in the measured temperature gradients from model to model, particularly when the gradients within a model are large.

Using the conductivity values at +10°C the scale of linear dimensions in Model #2 was established in accordance with the relation

$$\frac{L_2}{L_1} = \frac{K_2}{K_2} = \frac{0.35}{0.741} = 0.472$$

Since it was desired to maintain the same simulated contact conductance in Models #1 and #2, the PVC dimensions were established as follows:

$$C_1 = \left(\frac{k_1}{\ell_1}\right)_{PVC} = C_2 = \left(\frac{k_2}{\ell_2}\right)_{PVC}$$

since $k_1 = k_2$ (the PVC conductivity)

$\ell_1 = \ell_2$ for the PVC

The input power to the model heater was scaled as follows:

$$q_1^* L_1 = q_1/L_1^2 = q_2^* L_2 = q_2/L_2^2$$

thus $$\frac{q_2}{q_1} = \left(\frac{L_2}{L_1}\right)^2 = (0.472)^2 = 0.2228$$

where q - power input (watts)

q^* - power input per unit volume (watts/cm^3)

In summary, we would predict equivalent temperatures at identical geometric locations in Models #1 and #2 when the linear dimensions are scaled by a factor of 0.472, the lengths of the PVC insulator are equivalent, and the heater input powers are scaled by a factor of 0.2228.

The appropriate nominal input power to each model was established by considering the heat transport from surfaces (having an emittance of approximately one) of the model to an LN_2 temperature sink. The input power range and the model dimensions were established from the following criteria. First, the model size and re-radiating area was dictated by the size of the test chamber and it was desired to maintain temperature levels between +150 and -150°C to preclude damage to the surface coatings or the mechanical assembly. Second, it was desired to have a simple heat flow pattern as close to one-dimensional as possible, and yet have significant temperature gradients with the model. Preliminary hand calculations indicated that a power input range from 3 to 5 watts would be required for Model #1. Based on the above scaling laws the appropriate range for the 4130 model would be 0.67 to 1.1 watts. With these input ranges

established we chose the dimensions shown in Figure 1 for the two models.

The length of the PVC section (Part B of Figure 2) was established by considering the heat flow through the model. It was desired to choose a length which would produce a large gradient, such that the thermal resistance of the PVC section itself would be large by comparison to the resistance of the two joints. Temperature gradients in excess of 100°C were attained with a 3/4-inch long section of PVC.

C. MODEL FABRICATION

1. Materials

The Armco iron and SAE 4130 steel used in the models were checked for chemical composition by chemical and spectrographic analysis to insure that the "as received" material closely resembled the materials used in the thermal conductivity determinations published in References 1 and 2. The composition differences were extremely small and we concluded that the conductivities of the materials were representative of those measured. The analyses are presented in Appendix I.

The PVC portions of the models were machined from the same stock to minimize the chance of using materials with different conductivites for the simulated resistance member.

2. Joints

The PVC and metal sections were bonded together with a conductive epoxy[1] (silver-doped) which was applied according to the manufacturers recommendations. The use of this conductive epoxy was predicated on the need for a good thermal bond which would not introduce a significant resistance. A thin (0.005") layer was used for bonding the PVC to both the Armco and SAE 4130 parts.

During the first test with the Armco iron model the epoxy joint separated (in vacuum) when the temperature of the sample was allowed to fall to liquid nitrogen temperatures. This was apparently due to a difference in expansion coefficients of the materials forming the joint. Subsequently, we pinned the joints with a press fit using two 0.020" dia. stainless pins which were approximately 3/16-inch long. These pins added structural rigidity to the assembly without affecting the joint conductance. In all subsequent tests heater power was continuously supplied to prevent the joint temperature from reaching extremely low temperatures in the test chamber.

Concurrent with the testing of the thermal models a sample

---

1) Product of J. Waldman & Sons, Trenton, New Jersey.

joint of PVC and Armco iron was subjected to thermal shock tests (in air) at dry ice-acetone temperatures (approximately -80 C) and at liquid nitrogen temperatures. The joint sample was first inspected with a microscope to determine whether or not there were any cracks or joint imperfections. No imperfections were noted. The sample was then rapidly plunged into the dry ice-acetone bath, removed, allowed to warm-up to room temperature and then re-inspected. No apparent change in the joint surface was noted at a magnification of 40 X. A similar test was performed at liquid nitrogen temperatures and it was noted that the sample joint parted after the assembly was removed from the LN_2 and was warming up to room temperature. Microscopic investigations showed that the silver epoxy adhered to both the PVC and Armco iron and apparently the fracture occurred in the epoxy itself.

During the test program, using the two thermal models with pinned joints, we carefully inspected the surfaces of the joints before and after testing in vacuum. No apparent cracks or voids were observed even though the joint temperatures were subjected to temperatures as low as $-125^{\circ}C$. In this case, however, the temperature change from ambient was controlled and no thermal shocking could have occurred. Apparently a temperature environment in the vicinity of $-125^{\circ}C$ will not damage the joint (at low stress levels) whereas a liquid nitrogen temperature environment of $-196^{\circ}C$ may induce a failure in the epoxy bond.

3. Heater Elements

The heater elements were formed by winding resistance wire (#34 chromel-A for Model #1 and #36 Nichrome 5 for Model #2) around the periphery of the model. A layer of 1/2 mil Mylar was used to insulate (electrically) the heater wires from the model. After winding the resistance wire, a coat of insulating varnish was applied to the surfaces. The ends of the resistance wires were brought out of the multi-foil insulation as shown in Figure 1 and soldered to the heater leads after the insulation installation. After winding the heater, the ohmic resistance of the heater alone was accurately measured with a Wheatstone bridge. Tests with a sample of the heater wire at ambient, ice, and LN_2 temperatures indicated that the resistance changed by less than 1/2 percent. This change was not considered important in determining the true input power to the heater elements.

In Model #1, the heater lead wires were made from #32 manganin wire with a varnish insulation. This wire material was chosen because it has a low product of thermal conductivity and resistivity and therefore would tend to suppress heat leaks. Furthermore, manganin has a low temperature coefficient of resistivity and the lead wire resistance would be unaffected by the wire temperature.

In Model #2 the first tests were run with manganin lead wires; however, it was eventually discovered that heat leaks along the heater

lead wires were causing trouble in establishing a heat balance. This situation was created because of the low levels of input power (less than 1 watt). The final Model #2 configuration had 0.010-inch diameter pure nickel leads. The leads were not insulated and were mechanically polished with jewelers' rouge to decrease the surface emittance. The use of pure nickel reduced the I^2R losses in the leads to a small fraction of the total input power and the reduction in surface emittance minimized the heat leaks from the heater. A more complete description of these problems and their solution will be presented in Section III of this report.

4 Insulation

The insulation of the heater end of the model was accomplished by using multiple-layer insulations in which alternate layers of the insulation have low emittance surface characteristics. These thermal shields were separated by a low conductance glass paper to prevent thermal "shorts" from increasing the apparent conductivity. In vacuum systems, this type of insulation has a low apparent conductivity; however, extreme care must be taken in applying the insulation if it is desired to attain a low conductance with a minimum number of layers. In the present case it was desired to minimize the heat leaks from the heater section and the PVC member with a minimum amount of insulation.

Models #1 and #2 were insulated in a slightly different manner; however, the basic principle is shown in Figure 1. In Model #1, aluminum foil and Dexter paper (a glass paper product) were used to wrap the heater. Prior to completing this installation we received a quantity of 1/2 mil Mylar which we had gold coated on both sides. (The gold was applied by vapor deposition in vacuo to a thickness which rendered the material opaque). This material was used in place of the aluminum foil on subsequent installations since the use of this material reduces the problems associated with thermal short circuits at penetrations and joints.

The heater in Model #1 was insulated with five layers of insulation. Four layers of 4 mil thick Dexter paper alternated with 5 mil thick bright aluminum foil layers and a final wrap of a layer of Dexter paper and 1/2 mil gold-plated Mylar completed the installation. Extreme care was taken to fold the ends of the Dexter paper over the aluminum foil layers to prevent thermal "shorts". The final wrap was secured with a small amount of Eastman-Kodak 910 adhesive. "White glove" techniques were used in assembling the insulation to prevent the surfaces from being affected by handling. Model #2 was insulated with a continuous wrap of gold-plated Mylar and Dexter paper with a final cap of gold-plated Mylar over the end of the heater. During the test program two additional layers of insulation were added to this model in an attempt to reduce the heat leaks.

In both models the PVC section was insulated with an initial wrap of Dexter paper followed by two continuous wraps of Dexter paper and gold-plated Mylar.

Model #1 was supported by a nylon monofilament fish line (0.014-inch dia.) which penetrated the super-insulation layers. This arrangement subsequently caused some difficulty in Model #2. In the final tests of Model #2 we completely removed the support and suspended the apparatus by the thermocouple leads.

5. Thermocouples

Six thermocouples were attached to each model as shown in Figure 1. The thermocouple junctions were located along the center line and approximately equally spaced along the lengths of parts A and C. The locations, as shown in Figure 1, were numbered TC 1 and TC 7 and will herein be identified by these numbers.

The thermal models which were tested were relatively small, and therefore only small amounts of power were required to maintain their temperatures near the desired level. The installation of six thermocouples introduced a heat flow path from the model which became a significant fraction of the total re-radiated power. For example, the power input level to Model #2 was in the vicinity of one watt, and it was determined

that thermocouples alone could introduce a heat leak of 100 milliwatts or so if the leads acted as "long" fins. A sketch of the test chamber (which will be described in detail in a following section) and the thermocouple lead locations is shown in Figure 2. As shown, the leads passed through a small diameter neck in the LN_2 cooled vacuum chamber and radiated to a sink. Several methods for eliminating this heat leak problem were evaluated during the course of this program. They included:

a) The use of extremely small diameter thermocouple wire with a low emittance or insulated surface;

b) The use of thermistor-sensing elements attached with small diameter low conductivity lead wires;

c) The use of auxiliary heaters for each sensor lead to eliminate temperature gradients along the leads;

d) Scaling the instrumentation leads according to the thermal modeling laws.

After careful consideration of the simplicity of each method, we chose the latter as the one best suited to our tests.

Rather than scale the materials of the wires and the lengths, we treated the thermocouple leads as heat sinks and scaled the wire diameters such that the heat leak (at identical locations) per thermocouple in Model #2 would be approximately 0.22 that in Model #1. This, of course, is the same scale ratio as the heater power scale. For Model #2 we chose #40 AWG

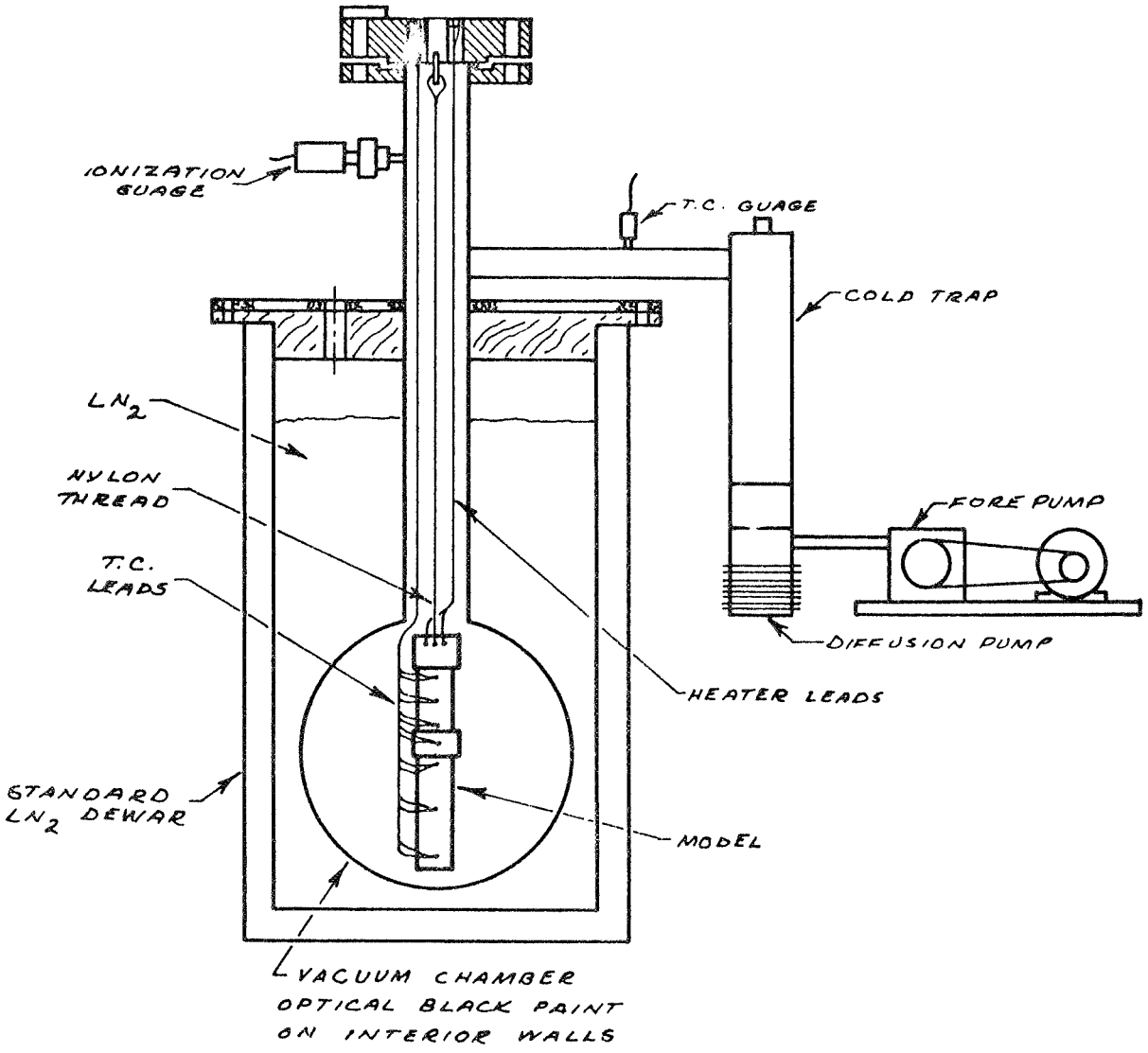

TEST CHAMBER ASSEMBLY

FIGURE 2

(5 mil) insulated wire as being the smallest practical (and readily available) size. On the basis of our scaling laws and an analysis of the heat leak through a typical wire, we determined that a #36 AWG wire of the same material would produce the approximate scale of power dissipation through the leads. The analysis is presented in Appendix II. It should be noted that we based our analysis on copper-constantan thermocouples. This effect of heat leaks could have been reduced by using wire materials of lower thermal conductivity (chromel-alumel, iron constantan); however, for reasons discussed in the following paragraph we choose copper-constantan for the experiments.

Copper-constantan thermocouple wire was selected for this application since this combination is easily assembled, has a favorable millivolt vs. temperature characteristic in the temperature range of interest, and, in general, this combination is relatively free from calibration corrections. Each thermocouple was referenced to $0^{o}C$ using constant level ice-water bath in a thermos bottle. The cold junctions were inserted in oil-filled glass tubes which were maintained at $0^{o}C$ by suspending the assembly of six tubes approximately 4 - 6" below the surface of the ice-water bath. A siphon system was used to maintain a constant bath level. Before attaching the thermocouples to the models, they were individually calibrated at $0^{o}C$ and $100^{o}C$ using an ice-water and a steam bath. The millivolt outputs were also obtained at dry ice-acetone and tap-water temperatures and compared with

readings from an etched stem precision glass thermometer. In all cases the thermocouple readings were within 1/2°C of the published (L & N) millivolt output vs. temperature data for copper-constantan.

The thermocouples were soft soldered (#35 Cera-Seal) into 1/16-inch diameter wells drilled into the thermal models. The leads were then cemented to the model with Pliobond cement and then taped to the model with a small strip of "Scotch" tape to prevent the leads from separating and producing erroneous temperature readings. The thermocouples in Model #1 were initially installed in the wells with "Ames" copper cement and the leads glued with Eastman 910 adhesive. During the first test in vacuum, several thermocouples separated when the model was temperature cycled. Subsequent testing was completed with the thermocouples soldered in place as described above.

Before installing the thermal models in the test chamber, the thermocouples were read out with the model at a uniform temperature (at ambient air temperatures) to check for uniformity. The results indicated that all thermocouples were reading within 1/4°C of each other.

6. Surface Coating

As previously discussed, it is necessary that the "basic" and scaled models have identical surface emittances when internal power is

dissipated by radiation. Previous experience in our laboratory indicated that "3M" brand Velvet Black Optical Coating[1] is relatively simple to apply, will adhere to most metals at low temperatures in vacuo and has a reproducible total hemispherical emittance close to unity. Emittances of 0.97 between LN_2 and ambient temperatures were measured in our laboratory. No apparent temperature dependence was noted. (This work was not performed under the subject contract).

The surfaces of Parts A and C of both models were coated with this paint. The metal surfaces were cleaned first with acetone, dipped into the paint and allowed to drip dry. After painting care was taken not to handle these painted surfaces. Note that the model measurements listed in Figure 1 apply to the measured dimensions before painting. After painting, additional measurements were made to determine the paint thickness. Approximately 0.0038-inch of paint was deposited on the surfaces.

The interior of the vacuum vessel shown in Figure 2 was also coated with this same paint to reduce internal reflections.

D. TEST EQUIPMENT

A schematic diagram of the test chamber is shown in Figure 2.

---

1) Manufactured by Minnesota Mining & Manufacturing Co.

The test chamber was a thin-walled stainless steel vacuum vessel having a 10 1/2-inch diameter spherical test section. A vacuum flange, sealed with an O-ring was mounted on the warm end of the neck of the vacuum vessel. The neck was a 2 1/2-inch diameter tube approximately 12 inches long. The lower portion of the neck and the spherical test section were submerged in liquid nitrogen contained in a 21-inch diameter LN_2 vacuum-jacketed dewar. By suspending the models in the approximate positions shown in Figure 2, the"black" surfaces of the models had a poor "view" of the warm end of the neck and the flange. The interior of the test chamber and the neck were coated with "3M" Optical black paint to minimize reflections.

The vacuum system consisted of a diffusion pump and LN_2 cold trap with a 15 CFM mechanical forepump. Several thermocouple gages and an ionization gage were used to read the chamber pressure during test. We experienced no difficulty with this vacuum system and after outgassing the model, (by heating),the pressures in the test section could be held at pressures down to 10^{-6} torr. In all of the test runs the pressure was below 10^{-5} torr. Two hermetic glass-to-metal seals were soldered in the flange to provide for thermocouple and heater lead throughs.

The thermocouples were referenced to $0^{\circ}C$ and the millivolt output read with a Minneapolis-Honeywell precision potentiometer. The thermocouples were each read and recorded at 1/2-hour intervals until the system

reached steady-state. A copper-constantan selector switch was used to conveniently read each location. The potentiometer could be read to within 5 microvolts which corresponds to approximate $0.1^{o}C$ at the temperature levels of interest. A 16-channel recording potentiometer was used to observe the cooldown period and to determine if there were any temperature fluctuations in the model temperatures. In all tests the temperatures were invariant once the model reached a steady-state condition.

The power input to the heater was supplied by a 0-50 VDC regulated power supply ($\pm$0.1 percent regulation). The voltage drop and the current flow to the heater were measured by a Weston precision voltmeter and milliammeter which were calibrated against laboratory standards. The power dissipated in the heater was calculated from measurements of the current flow and the actual resistance of the heater. This method was selected since measurements of the voltage drop at the heater itself would require additional leads and would introduce another source for heat flow.

III. TEST RESULTS

In the following section we will present the results of the thermal tests which were undertaken in the test apparatus shown in Figure 2. The first tests were performed with the "basic" model fabricated of Armco iron. The dimensions and configuration are shown in Figure 1. We discussed previously that the first run with this model was unsuccessful due to the fact that the epoxy joint separated during testing when the model temperature was allowed to fall to liquid nitrogen temperatures. This occurred during a shutdown of the heater. The model was subsequently repaired and the joint pinned (see Section II for details). The test results for this Armco iron model configuration are presented in Table I. The tests were run at four input power levels, and at each power level the model was allowed to reach thermal equilibrium. The measured temperatures represent this steady-state condition. The temperature subscripts are referenced to the thermocouple locations shown in Figure 1.

In Table I the heater input power was computed by subtracting the I^2R losses in the heater leads from the measured total input power; the correction being approximately 5 percent of the total input power. In the true physical situation the heater leads themselves act as potential heat sources or sinks, and can influence the true input power to the model. Although the terminal temperatures of the leads were at approximately the same temperature, the heat flow in the lead wires is dominated by the internal power dissipation and the radiation interchange between the leads

TABLE I

THERMAL MODELING TEST DATA - RUN #2

Thermal Model #1 - Armco Iron, k = 0.741 watt/cm^{o}K at 10^{o}C with PVC insulator
Manganin heater lead resistance 18.92 ohms
Copper-constantan thermocouples - reference junction 0^{o}C (#34 AWG)
Sample container pressure $\leq$ 1 x 10^{-5} torr
Sample container wall temperature 77^{o}K
0.014" nylon monofilament support thread

Date	Voltage (volts)	Current (m. amps)	Input Power (watts)	Heater Power (watts)		Temperature (^{o}C)
9-4-62	44.0	115	5.060	4.810	T_1	-115.6
"					T_2	-114.9
"					T_3	-113.7
"					T_5	70.5
"					T_6	74.8
"					T_7	86.3
9-1-62	35.9	93.9	3.371	3.204	T_1	-124.2
"					T_2	-123.4
"					T_3	-122.9
"					T_5	35.9
"					T_6	36.6
"					T_7	46.9
8-31-62	41.9	109	4.567	4.342	T_1	-116.1
"					T_2	-115.1
"					T_3	-114.0
"					T_5	61.3
"					T_6	64.3
"					T_7	75.9
8-31-62	44.8	116.5	5.219	4.962	T_1	-113.2
"					T_2	-112.5
"					T_3	-111.2
"					T_5	72.5
"					T_6	76.5
"					T_7	88.9

and the neck of the test chamber. To determine the value of the temperature gradient (and therefore the heat flow) at the heater end of the leads it would be necessary to solve a complex heat flow problem since the lead wire "views" a non-uniform temperature environment in the neck of the test chamber. Furthermore, the temperature of lead wire at the heater end is unknown, and a thermoccuple measurement would introduce another potential heat leak. We recognized this difficulty in correctly estimating the true input power and contemplated using an additional heater to maintain the lead at a uniform temperature. This approach was not used because of the added complexity involved. In view of these problems we calculated the power dissipated from the model using the measured temperature distributions and found that the heat balance agreed with the calculated heater input power within a few percent. For Model #1 an uncertainty in the input power measurement of $\pm$ 1 percent will introduce an uncertainty of $\pm 0.75^{\circ}C$ in the mean temperature of the model between the heater and the PVC section. A comparison of the re-radiated power and the calculated input power for this model and Model #2 will be presented in a following discussion.

The measured temperatures for Model #1 are plotted in Figure 3 as a function of the model length measured from the heater end. The gradients in the Armco iron at the heater end vary from 11 to $16^{\circ}C$ whereas the gradients in the Armco iron member (Part C) at the extreme end are only several degrees. The gradient across the PVC insulator was of the order of 160 to 180 C.

MEASURED TEMPERATURE DISTRIBUTION
RUN # 2 MODEL # 1

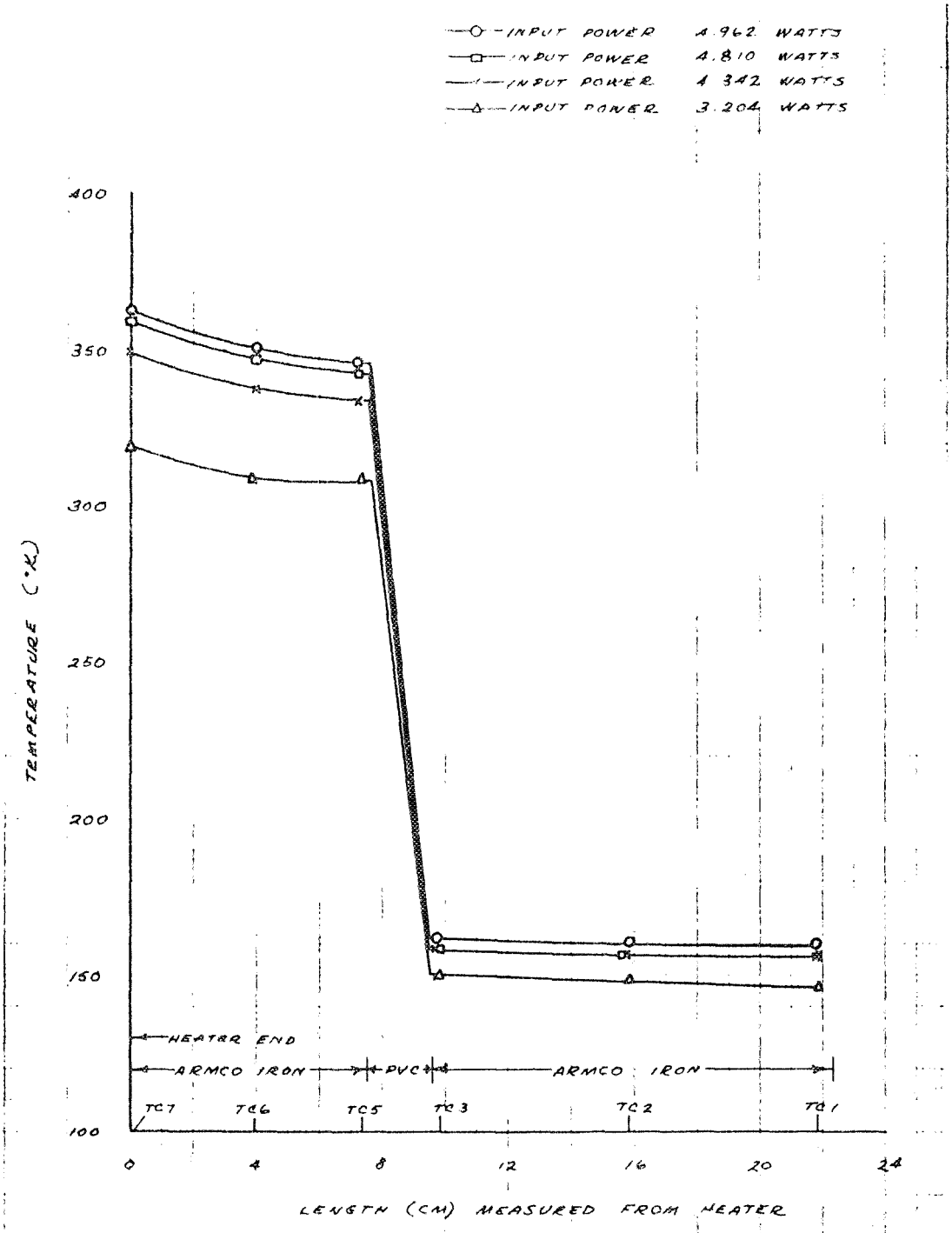

FIGURE 3

The test data for Model #2 are presented in Tables II, through V. In Table II the data were obtained with manganin heater leads similar to those used for Model #1. The tabulated values of the heater power were calculated from the current flow and the resistance of the heater winding itself. The tabulated values of the "scaled" power input were obtained by multiplying the heater input power by the scale factor of 4.488. This scale factor is based on the thermal modeling laws and is derived in Section II. Thus, the temperature distributions in Models #1 and #2 should be identical when the heater input power in Model #1 is equivalent to the "scaled" heater input power in Model #2.

Comparing Tables I and II it can be seen that the temperatures of Model #2 between the heater and PVC insulator were considerably less than measured temperatures of Model #1 at scaled input powers. For example, at a scaled input power of 3.23 watts the temperatures were low (in this region) by 5 - 10^{o}C. The temperatures at locations 1, 2 and 3 were approximately 5 to 6^{o}C higher than Model #1, indicating that more heat was flowing through the PVC insulator. It should be noted that small differences in the amount of heat flowing in the insulator cause large differences in the mean temperature of Part C. At this input power level, for example, the sensitivity of the mean temperature at the heater end is 0.12 ^{o}C/milliwatt whereas the sensitivity of the mean temperature of the extreme end of the model is 0.63 ^{o}C/milliwatt. This means that an uncertainty

TABLE II

THERMAL MODELING TEST DATA - RUN #3

Thermal Model #2 - SAE 4130 (k = 0.35 watt/cm^{o}K at 10^{o}C) with PVC insulator
Manganin heater lead (#32 wire)
Copper-constantan thermocouples - reference junction 0^{o}C (#40 AWG)
Sample container pressure $\leq$ 1 x 10^{-5} torr
Sample container wall temperature 77^{o}K
0.014" nylon monofilament support thread

Date	Voltage (volts)	Current (m. amps)	Heater Power (watts)	Scaled Heater Power (watts)		Temperature (^{o}C)
9-10-62	14.4	76.0	0.9871	4.43	T_1	-112
"					T_2	-112
"					T_3	-110
"					T_5	+ 55
"					T_6	+ 57
"					T_7	+ 63
9-8-62	13.6	71.0	0.872	3.91	T_1	-113
"					T_2	-113
"					T_3	-111
"					T_5	+ 47
"					T_6	+ 49
"					T_7	+ 54
9-10-62	12.3	65.0	0.721	3.23	T_1	-118
"					T_2	-117
"					T_3	-115
"					T_5	+ 29
"					T_6	+ 31
"					T_7	+ 35

TABLE III

THERMAL MODELING TEST DATA - RUN #5

Thermal Model #2 - SAE 4130 with PVC insulator

Note: All conditions as Run #3 except manganin leads replaced with polished nickel leads (0.010" dia.)

Date	Voltage (volts)	Current (m. amps)	Heater Power (watts)	Scaled Heater Power (watts)		Temperature (^{o}C)
9-15-62	11.0	66	0.720	3.23	T_1	-121
					T_2	-120
					T_3	-118
					T_5	+ 34
					T_6	+ 36
9-15-62	11.0	66	0.720	3.23	T_7	+ 40

TABLE IV

THERMAL MODELING TEST DATA - RUN #8

Thermal Model #2 SAE 4130 with PVC insulator

Note: All conditions similar to Run #5 except 0.014" nylon support thread replaced with 0.0075" nylon. One additional wrap of super insulation added to heater area. Removed TC 2 and relocated between TC 7 and TC 6.

Date	Voltage (volts)	Current (amps)	Heater Power (watts)	Scaled Heater Power (watts)		Temperature (^{o}C)
10-25-62	11.0	66	0.720	3.23	T_1	-117
					T_3	-115
					T_5	+ 33
					T_6	+ 35
					T_2	+ 37
10-25-62	11.0	66	0.720	3.23	T_7	+ 40

TABLE V

THERMAL MODELING TEST DATA - RUN #9

Thermal Model #2 - SAE 4130 with PVC insulator

Removed nylon support. Thread and suspended model by thermocouples. Added additional wrap of "super" insulation at heater end.

Date	Voltage (volts)	Current (m. amps)	Heater Power (watts)	Scaled Heater Power (watts)		Temperature (^{o}C)
9-26-62	12.95	77	.980	4.398	T_1	-110.5
					T_3	-108.7
					T_5	62.1
					T_6	64.8
					T_2	67.0
					T_7	72.6
9-27-62	11.05	66	.720	3.232	T_1	-117.3
					T_3	-115.9
					T_5	37.0
					T_6	38.8
					T_2	40.3
					T_7	43.9
9-27-62	13.6	81	1.085	4.870	T_1	-109.3
					T_3	-107.6
					T_5	71.4
					T_6	74.3
					T_2	76.5
					T_7	81.8

of 10 milliwatts in the heat flowing through the PVC insulator is reflected in a 6°C change in T_2. We state this example to show the difficulties which one encounters in thermal testing when the temperature levels are low and the dissipated flux is small.

A heat balance for this run indicated that the re-radiated power was considerably less than the measured heater input. We felt that the heat leak along the heater leads was a potential source of trouble and replaced the manganin leads with pure nickel un-insulated leads. Although nickel has a higher thermal conductivity than manganin we were able to highly polish the surface of the nickel leads and thereby reduce the surface emittance. A low emittance would tend to reduce the heat leak from the wire.

The data for this configuration are presented in Table III. It should be noted, however, that the model was not in complete equilibrium. The data were obtained when T_1, T_2 and T_3 were increasing in temperature, and these tabulated values are low. The remaining temperatures were in equilibrium, (the time constant for this end being much smaller than the extreme end where the mean temperature level is lower). The values indicate that the mean temperatures at the heater end were increased by approximately 5°C; however, they were below those measured for Model #1.

Another test run was made with a smaller diameter support cord (0.0075" dia.) and an additional wrap of insulation on the heater. As shown in Table IV the mean temperatures did not appear to be affected by this change. In this run TC 2 was relocated between TC 7 and TC 6 to obtain a better picture of the gradients at the heater end.

Although we did not note any apparent change in the temperatures in Run #8, we still suspected that this support penetration in the insulation was a source of heat leakage. In Run #8 the mean temperatures of the heater end of the model were low by some 5°C, and a heat leak of some 40 milliwatts would represent this difference.

The next test with Model #2 was made with the nylon support completely removed, and an additional wrap of insulation on the heater. The data for this run are presented in Table IV and plotted in Figure 4. Comparing Tables III and IV it can be seen that the heater end temperatures increased by approximately 3°C due to the removal of the penetration.

A comparison of the temperature data for Models #1 and #2 is presented in Figure 5. In this plot the dimensions of Model #2 were scaled by the conductivity ratio of the Armco iron and SAE 4130. Similarly, the input powers were scaled for comparative purposes. Data are presented for two input power levels where the mean temperature was increased by

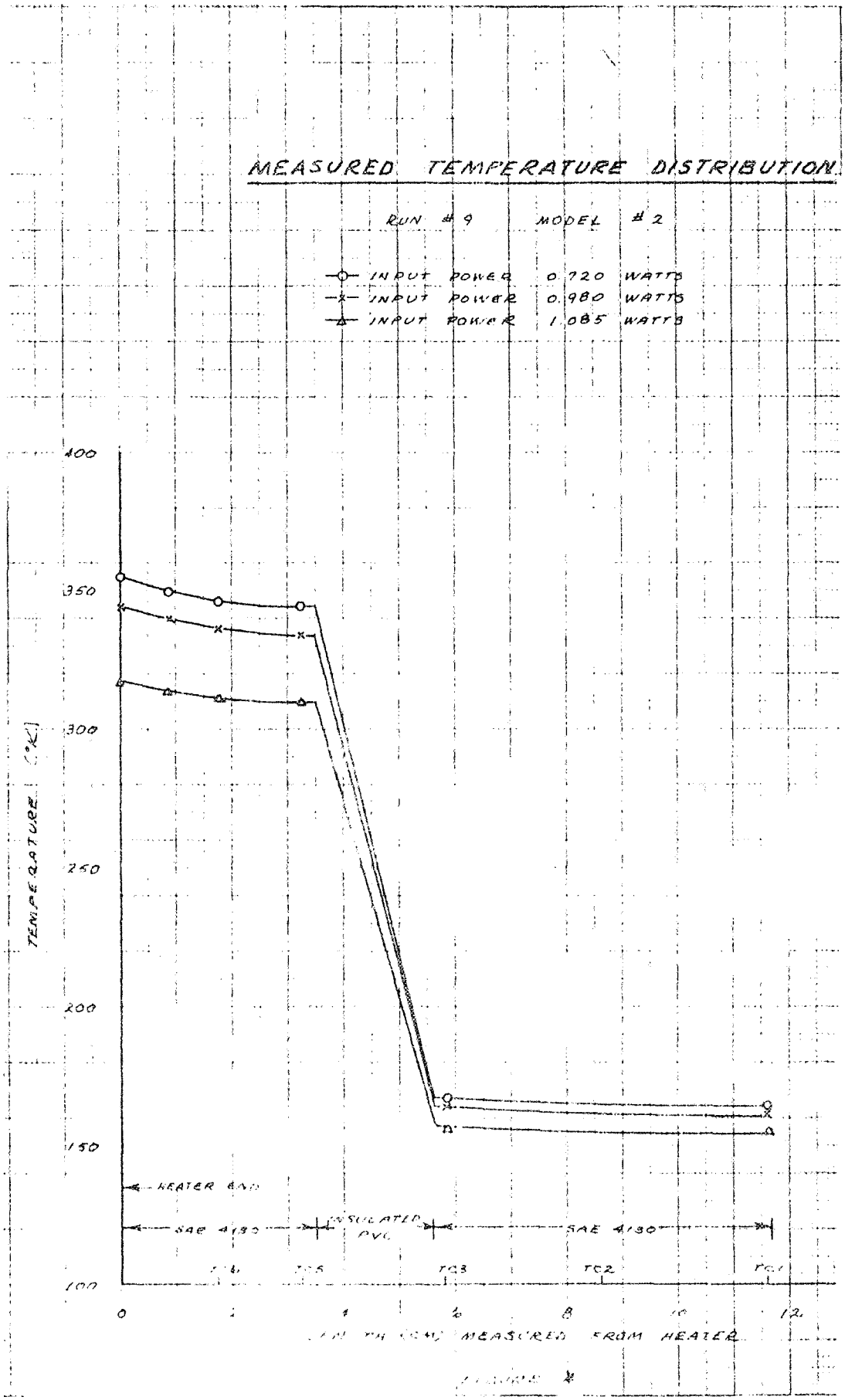
MEASURED TEMPERATURE DISTRIBUTION
RUN # 9 MODEL # 2
INPUT POWER 0.720 WATTS
INPUT POWER 0.980 WATTS
INPUT POWER 1.085 WATTS
TEMPERATURE (°K)
400
350
300
250
200
150
100
HEATER END
SAE 4130
INSULATED PVC
SAE 4130
TC6
TC5
TC3
TC2
TC1
0
4
8
12
MEASURED FROM HEATER

COMPARISON OF TEMPERATURE DISTRIBUTIONS AT IDENTICAL GEOMETRIC LOCATIONS

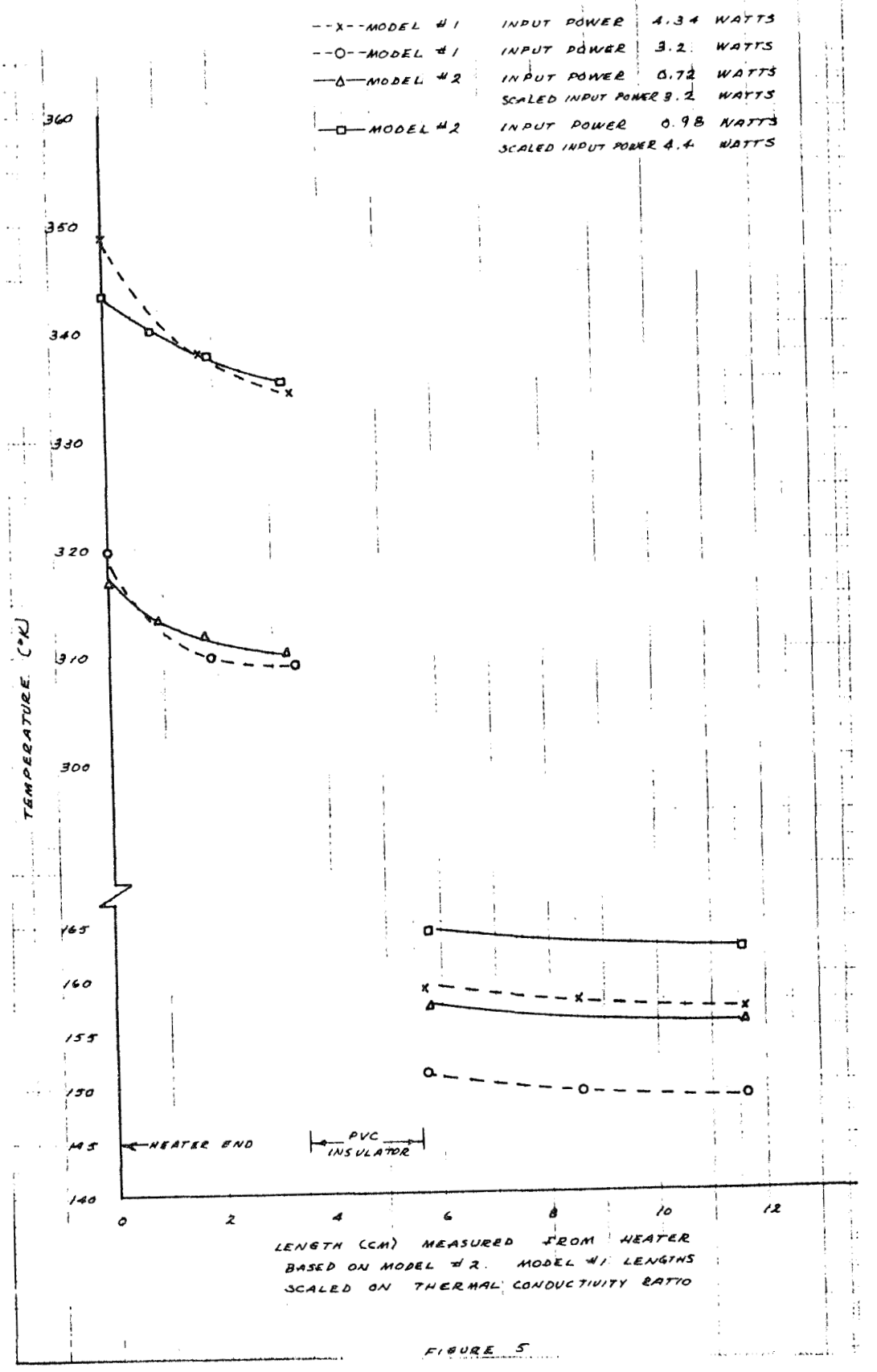

FIGURE 5

approximately 30°C. As shown in Figure 5, the heater end temperatures scaled to within 3°C at the lower power level and within 3.3°C at the higher power level. Note that the temperature gradient at the heater end of Model #1 becomes significantly greater than that measured for Model #2 as the mean temperature level is increased. We believe that part of this discrepancy can be traced to the fact that the conductivity of the Armco iron decreases with increasing temperature more than the SAE 4130. This would,of course, change the appropriate scaling factors for the two models. Our scaling ratio was calculated for a mean temperature of +10°C which is lower than either of the plotted curves. This effect is shown more clearly in Figure 6 where T_7 and T_6 are plotted for both models as a function of input power.

The scaled temperatures at the extreme end of the model indicate a difference of between 5 and 7°C (an error of some 4 percent in absolute temperature). In this case we would attribute some of the discrepancy to the simulations of a joint conductance, since these temperatures are extremely sensitive to the heat flowing in the PVC member.

In Table VI we have compared the temperature distributions in the two models with an IBM 7090 computer solution. (The computer program was developed at Arthur D. Little, Inc., to solve for the transient temperature distributions in spacecraft and was available for this solution). In this analytical solution, we estimated the conductance of the PVC member

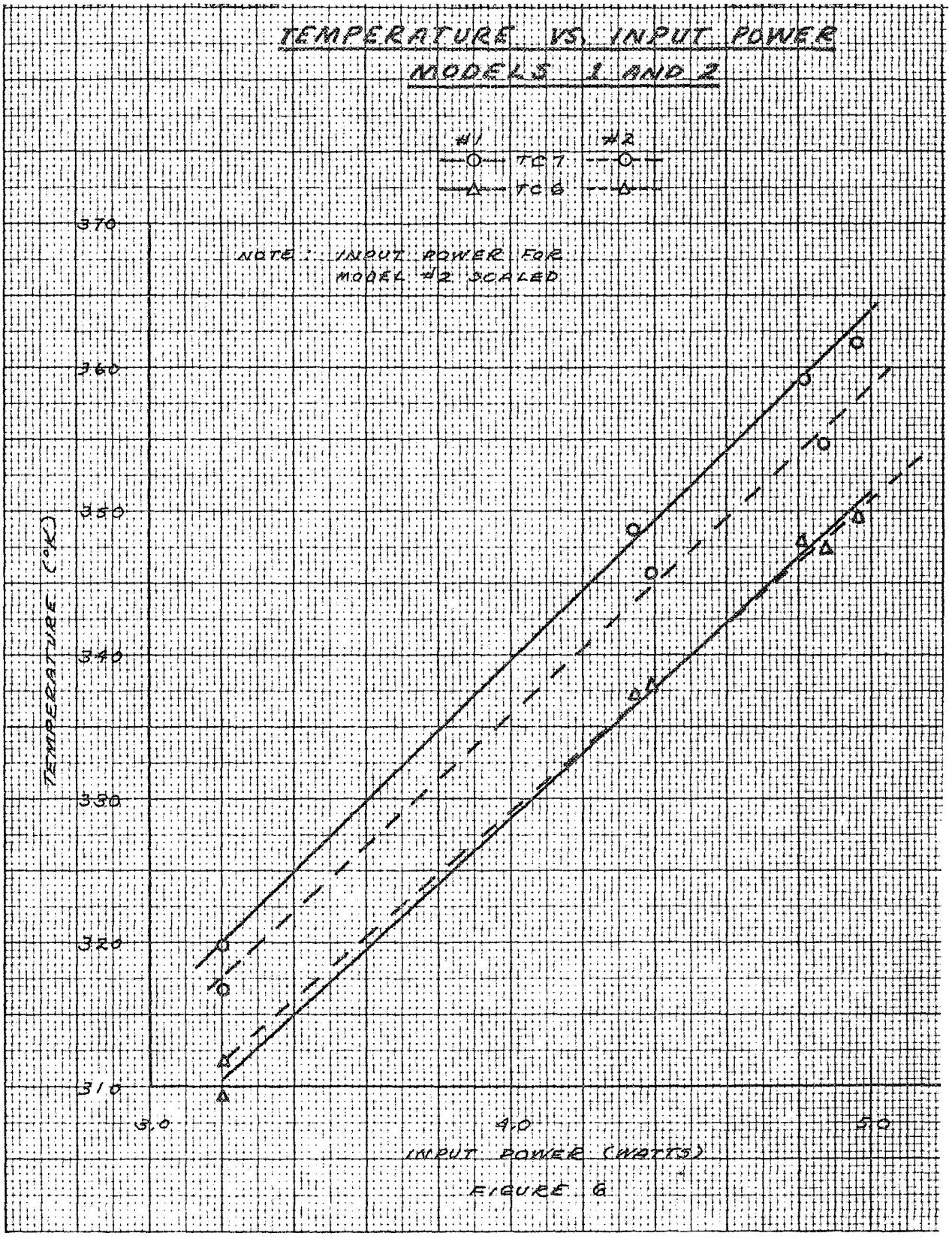
TEMPERATURE VS. INPUT POWER
MODELS 1 AND 2
#1
#2
TC 7
TC 6
NOTE: INPUT POWER FOR MODEL #2 SCALED
370
360
350
340
330
320
310
TEMPERATURE (°K)
3.0
4.0
5.0
INPUT POWER (WATTS)

FIGURE 6

TABLE VI

COMPARISON OF MACHINE CALCULATIONS AND MEASURED TEMPERATURES

(All temperatures in ^{o}K)

Power input to heater 4.0 watts

	Machine Calculations	Model #1	Model #2
TC 1	158.5	154	160
TC 2	159.3	155	
TC 3	160.7	156	162
TC 5	320.0	327	327
TC 6			
TC 7	334.9	340	336

based on a published thermal conductivity value of 0.003 watt/cm^{o}K. Since we did not measure the thermal conductivity, and the "k" for plastic materials can vary from lot to lot by a factor of 2 or more, we regard these calculations as merely indicative of the temperature ranges. In the machine calculation we accounted for the thermocouple heat leaks by treating each lead location as a heat sink. The heat flow was estimated using the procedures developed in Appendix II of this report. An emittance of 0.97 was assumed. It was also assumed that no heat flowed through the super insulation surrounding the heater or PVC. Referring to Table VI, it can be seen that the temperatures are in fair agreement, with the calculated heater end temperatures lower than those measured.

In Table VII we have tabulated the re-radiated power and the apparent joint conductance for each model at different power levels. The re-radiated power was obtained by computing the mean intensity of the thermal radiation leaving each of the two radiating surfaces, (Parts A and C in Figure 1). The measured temperatures were used to establish the T^4 distribution. The mean intensity was found by numerical integration using Simpson's rule. An emittance of 0.97 was assumed. In this calculation we accounted for the radiant interchange between the model and the LN_2 temperature walls of the test chamber. A uniform temperature of 77^{o}K was assumed. In all of the Model #2 tests the re-radiated power was one to two percent less than the computed heater input power. The computed re-radiated power for Model #1 was less than the heater power for two power levels and

TABLE VII

COMPARISON OF HEAT BALANCES AND JOINT CONDUCTANCES

Run	Model	Heater Power (watts)	Re-radiated Power (watts)	% Deviation	Apparent joint Conductance watts/cm^2 ^oK
2	1	3.204	3.0797	-3.88	1.02×10^{-3}
2	1	4.342	4.3119	-0.69	1.16×10^{-3}
2	1	4.810	4.8234	+0.28	1.11×10^{-3}
9	2	.720	0.7046	-2.13	1.30×10^{-3}
9	2	.980	0.9633	-1.70	1.37×10^{-3}
9	2	1.085	1.0693	-1.45	1.36×10^{-3}

slightly greater for the highest power level. In this table the deviation is referenced to the calculated heater input power.

The calculated re-radiated power was less than input power indicating that the effect of thermocouple heat leaks was significant. Note that the largest deviation represents a difference of only 120 milliwatts. A significant fraction of this deviation could be attributed to thermocouple heat leaks. We conclude that the heat balances are within a reasonable degree of accuracy considering the fact that variations in the surface emittances, insulations, leaks, and the heat flow in the instrumentation connections lead to uncertainties of this magnitude.

The apparent joint conductance was computed from the measured temperature drop across the PVC insulator, and the net heat flow dissipated by the end of the model (Part C of Figure 1). In addition, we accounted for the heat leak through the thermocouples using the method derived in Appendix II. The apparent conductance was obtained from the expression

$$C = \frac{Q_r + Q_T}{A\Delta T}$$

where Q_r - net power radiatively dissipated by Part C

Q_T - thermocouple heat leak (calculated)

A - cross-sectional area of model

ΔT - temperature drop across the PVC as measured by $T_5 - T_3$

It should be noted that the correction for the thermocouple losses is only approximate; however, this loss was estimated as approximately 8 percent of the re-radiated power. From Table VII it can be seen that the apparent joint conductance of Model #1 was computed to be lower than Model #1; however, for a given model the computed conductances did not vary by more than 12 percent. If we compute an average apparent joint conductance the maximum deviation of the computed values is approximately $\pm$15 percent. We investigated the magnitude of this deviation by computing an uncertainty interval for the apparent conductance based on estimates of the accuracy of the temperature readings and an estimate of the uncertainty interval of the emittance. Assuming that the temperatures were measured to within $1^{o}C$, and the emittance was 0.97 ± 0.01, we calculated that the most probable uncertainty in the joint conductance for a given model would be 0.10×10^{-3} watts/$cm^{2o}K$. This uncertainty alone is approximately 10 percent which is the same order of magnitude as the spread in the data. In comparing the joint conductances of Models #1 and #2, one must add in the uncertainties involved in the scaling process.

APPENDIX II

THERMOCOUPLE SCALING

Consider the case of a thermocouple wire which acts like a "long" fin. One end is maintained at T_o, i.e., at the model,and the wire is losing heat by radiation to a low-temperature sink. If we neglect any re-radiation from the surrounding sink, the heat flow along the wire length (assuming that radial gradients are small) is given by the expression

$$-k A_c \frac{d^2T}{dx^2} + p \epsilon \sigma T^4 = 0 \qquad \text{II-1}$$

where A_c - cross-sectional area

p - perimeter

This equation can be integrated once to yield

$$q = -k A \left.\frac{dT}{dx}\right|_{x=o} = \sqrt{2/5\ p \epsilon \sigma T_o^5\ k A_c} \qquad \text{II-2}$$

This is the heat loss from the end of a rod whose end temperature is T_o.

In the actual case of insulated thermocouple leads it can be shown that the temperature gradient from the inner copper or constantan wire to the outermost surface is less than a degree for nylon or fiberglass insulation when the ratio of the O.D. to the wire diameter is approximately 6 and the mean temperature is in the vicinity of 0^oC. The perimeter in Equation II-2 is thus based on the O.D. of the insulation. Furthermore,

it can be shown that the conduction along the lead is governed by the conductance of the wire rather than the insulation. Thus, the cross-sectional area for heat flow is based on the wire diameter, and the conductivity in Equation II-2 is that of the wire material.

In Models #1 and #2 the thermocouples were made of identical wire materials, had the same insulation and therefore approximately the same emittance, and at identical geometric locations would have the same temperatures. In this case the ratio of the heat leaks along the thermocouple leads in Models #1 and #2 is given by the expression

$$\frac{q_2}{q_1} \propto \sqrt{\frac{(D_o\ D_i^2)_2}{(D_o\ D_i^2)_1}} \qquad \text{II-3}$$

where

D_o - insulation O.D.

D_i - wire diameter

subscripts 1, and 2 refer to Figure 1 nomenclature

The thermocouple lead dimensions were:

Model #1 $D_o = 0.024"$, $D_i = 0.005"$

Model #2 $D_o = 0.0045"$, $D_i = 0.0038"$

With these values

$$\frac{q_2}{q_1} = 0.33$$

Using the thermal conductivity of Models #1 and #2 we calculated that the ratio of input powers (or losses) would be 0.223, (c.f. Section II-2). The thermocouples are therefore not exactly scaled (since we could not find leads with the appropriate dimension); however, since the heat leaks are small we would consider the difference in the scale factor as having a minor effect on the temperature distribution.

Based on the measured thermocouple dimensions of Model #1 we calculated the total heat leak per thermocouple (for a copper and a constantan lead) as a function of the end temperature using Equation II-2. (The emittance was assumed to be 0.9, k = 4.0 watts/cm^{o}K for copper and k = 0.25 watts/cm^{o}K for constantan).

T_o (K)	q_1 (milliwatts)	q_2 (milliwatts)
300	27	9
200	10	3.3

REFERENCES

1. Thermal Conductivity of Metals and Alloys at Low Temperatures, NBS Circular 556, September 1954.

2. Powell, et. al., Armco Iron as a Thermal Conductivity Standard, Progress in International Research on Thermodynamic Properties, ASME Publication, June 24, 1962.